Korean J. Chem. Eng., 37(3), 571-575 (2020)
DOI: 10.1007/s11814-020-0475-8

pISSN: 0256-1115
eISSN: 1975-7220

Facile synthesis of mesoporous Cr_2O_3 microspheres by spray pyrolysis and their photocatalytic activity: Effects of surfactant and pyrolysis temperature

The Ky Vo* and Jinsoo Kim,†**

*Department of Chemical Engineering, Industrial University of Ho Chi Minh City,
12 Nguyen Bao, Go Vap, Ho Chi Minh City, Vietnam
**Department of Chemical Engineering, Kyung Hee University,
1732 Deogyeong-daero, Giheung-gu, Yongin-si, Gyeonggi-do 17104, Korea
(*Received 16 November 2019 • accepted 25 December 2019*)

Abstract−Mesoporous Cr_2O_3 microspheres with improved pore structure were prepared by spray pyrolysis method. A precursor solution was nebulized into fine droplets containing chromium salt and cetyltrimethylammonium bromide (CTAB), which were then pyrolyzed to Cr_2O_3/C_x microspheres inside a tubular furnace, followed by post-heat treatment to eliminate the carbonaceous material. The produced Cr_2O_3 particles had a diameter of 0.5-1 μm and their textural properties could be tuned by adjusting CTAB amount and pyrolysis temperature. The synthesized Cr_2O_3 microspheres had the highest surface area and pore volume of 52 m^2 g^{-1} and 0.3 cm^3 g^{-1}, respectively, which surpass those of Cr_2O_3 prepared using a conventional method such as thermal decomposition, hydrothermal reduction or wet chemical synthesis. The photocatalytic degradation of methyl orange dye (MO) was tested on the prepared Cr_2O_3 particles. It was determined that the spray pyrolysis-derived Cr_2O_3 exhibited greater photocatalytic activity than that of commercial TiO_2 and Cr_2O_3 particles prepared by the thermal decomposition of chromium salt.

Keywords: Spray Pyrolysis, Mesoporous Cr_2O_3 Microsphere, CTAB, Methyl Orange Degradation, Photocatalyst

INTRODUCTION

Mesoporous metal oxides with high specific surface area and large pore volume have attracted considerable interest in many application fields such as lithium ion batteries, sensors, supercapacitors, and catalysts [1,13,20,25,28,31]. Chromium oxides (Cr_2O_3) are some of the most important metal oxides. Nanostructured Cr_2O_3 particles have been widely used as pigments, coating materials, and catalysts [11,19]. In the field of catalysis, Cr_2O_3 has been used in many reactions, such as water-gas-shift reaction [16], dehydrogenation [4], hydrogen sorption [21], gas sensors [13] and a photocatalysts [14,24,32]. Thus far, various approaches have been developed to prepare Cr_2O_3 particles, including hydrothermal reduction [18], solution combustion [12], sonochemistry [9], and microwave plasma application [30]. It has been reported that mesoporous chromium oxide can be prepared with or without template materials (hard template and soft template). Valdes et al. [27] used silica and carbonaceous materials as hard templates to prepare mesostructured Cr_2O_3. Bai et al. [3] prepared hollow Cr_2O_3 microspheres using the yeast bio-template route. The template-free synthetic approach has been widely used to prepare metal oxides. Chen et al. [5] synthesized mesoporous spherical Cr_2O_3 using the hydrothermal method by controlling the morphological evolution. Roy et al. [22] prepared Cr_2O_3 nanocubes by solvothermal synthesis without a template. In general, these approaches can be applied on a laboratory scale to produce small amounts of products. Large-scale production of chromium oxide (or metal oxides in general) requires a cost-effective approach. The synthesis of metal oxides by spray pyrolysis has been considered as a promising approach because it allows production of large quantities of materials in a short reaction time as it is a continuous flow process. Cho et al. [6] prepared the $Gd_2O_3:Eu^{3+}$ yolk-shell structure by spray pyrolysis. Yoon et al. [7] synthesized MoO_3 nanoplates by ultrasonic spray pyrolysis. In our previous studies, we prepared TiO_2 [8] and Mo/Al_2O_3-TiO_2 [29] in a short reaction time by spray pyrolysis. The results showed that the obtained metal oxide microspheres had mesoporous structures with a higher surface area and a larger pore volume compared to those of commercial products. In addition, the products derived by spray pyrolysis showed greater catalytic activity than those of commercial products [8,29], which demonstrates their considerable potential application in chemical industry owing to their relative cost effectiveness and versatility [26]. To our knowledge, there have been no reports on mesoporous Cr_2O_3 prepared by spray pyrolysis.

In this study, mesoporous chromium oxide (Cr_2O_3) microspheres with improved pore structures were prepared by the one-step spray pyrolysis method. During the spray pyrolysis, the spherical Cr_2O_3 particles were quickly formed from the droplets containing a chromium salt solution. To enhance the porosity of the produced Cr_2O_3, cetyltrimethylammonium bromide (CTAB) was used as a mesoporous template agent. The effects of CTAB and pyrolysis temperature on the characteristics (e.g., morphology, particle size, porosity, and crystallinity) of the prepared Cr_2O_3 were investigated. The obtained Cr_2O_3 particles were tested for the photocatalytic degradation of a methyl orange (MO) dye in an aqueous solution.

†To whom correspondence should be addressed.
E-mail: jkim21@khu.ac.kr

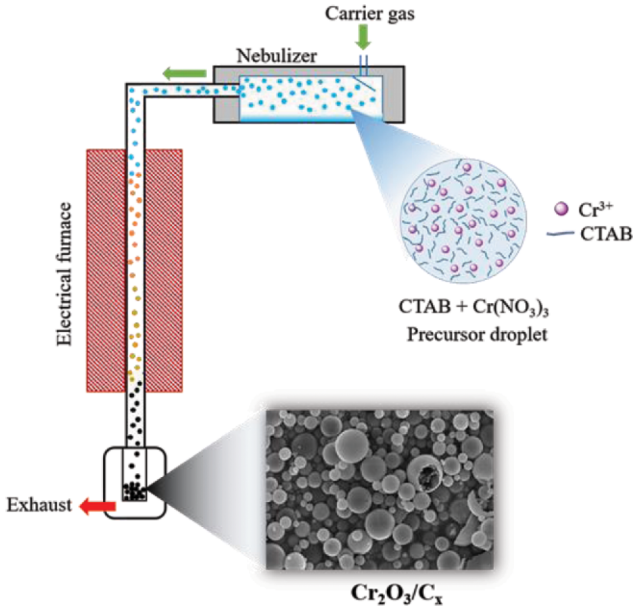

Fig. 1. Schematic diagram of the Cr_2O_3 preparation by the spray pyrolysis system.

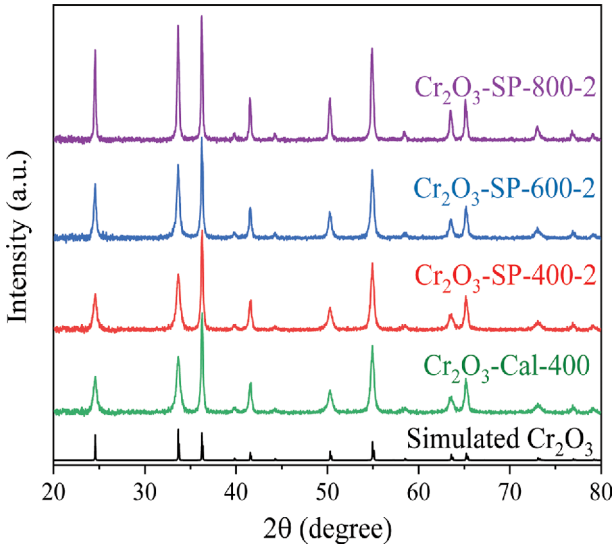

Fig. 2. XRD patterns of Cr_2O_3 samples prepared by different methods and synthesis conditions.

EXPERIMENTAL

1. Synthesis of Cr_2O_3

Precursor solution for spray pyrolysis was readily prepared by dissolving 17 g of $Cr(NO_3)_2 \cdot 9H_2O$ (Sigma-Aldrich) in 250 mL of deionized water to obtain a 0.2 M solution, followed by the addition of the calculated amount of CTAB under vigorous stirring for 2 h. Then, the mixed solution was directly used for spray pyrolysis by a 1.7 MHz ultrasonic spray generator to produce fine liquid droplets, which were then carried into a quartz reactor maintained at a desired temperature by a constant flow N_2 gas of 6 L min^{-1}. The produced particles were collected in a Teflon bag at the bottom of the spray pyrolysis unit (Fig. 1). Post-heat treatment was performed by heating the obtained product at 400 °C for 4 h at a heating rate of 2 °C/min in the air. The produced samples are denoted as Cr_2O_3-SP-X-Y, where X is the pyrolysis temperature (400-800 °C) and Y is the CTAB/Cr^{3+} molar ratio (0-2). We determined that the use of a higher CTAB amount (CTAB/Cr^{3+}>2) resulted in a solution with a relatively high viscosity, which cannot be nebulized under ultrasonic spray conditions. For comparison, the Cr_2O_3 powder was conventionally prepared by the thermal decomposition of chromium salt at 400 °C for 4 h in the air, and the resulting sample was denoted as Cr_2O_3-Cal-400.

2. Characterization

The phase structure and crystallinity of the prepared samples were investigated by X-ray diffraction (XRD; Miniflex 600, Rigaku, Japan) with a Cu Kα radiation source (λ=1.54 Å). SEM images were obtained by field-emission scanning electron microscopy (FE-SEM; Leo-Supra 55, Carl Zeiss STM, Germany). FT-IR spectra were collected by an FT-IR spectrometer (Tensor 27, Bruker, Germany). The BET surface area and pore structure of the samples were analyzed using N_2 porosimetry (Tristar 3020, Micromeritics, USA). Before each measurement, the sample was degassed at 150 °C for 6 h under vacuum.

3. Photocatalytic Activity

The photocatalytic activity of the synthesized Cr_2O_3 sample was investigated by measuring the degradation of methyl orange in an aqueous solution under ultra-violet (UV) light. For each run, 0.1 g of Cr_2O_3 was first dispersed in 100 mL of the MO solution (15 mg/L) under vigorous stirring and sonication. The resulting suspension was irradiated with UV-light emitted from a 400 W mercury lamp under continuous stirring. A circulating water bath was used to maintain the reaction temperature at 25 °C. The concentration of MO in the reaction mixture was analyzed at a certain interval time by UV-visible spectrophotometry (Optizen POP, Mecasys, Korea).

RESULTS AND DISCUSSION

Fig. 2 shows the PXRD patterns of the Cr_2O_3-Cal and Cr_2O_3-SP samples. The XRD patterns of all samples show well-crystallized phases, and the characteristic diffraction peaks of the prepared samples match well with those of the simulated pattern of pure rhombohedral phase Cr_2O_3 (JCPDS Card no. 38-1479). With an increase in the pyrolysis temperature from 400 °C to 800 °C, the XRD peak intensities increased because higher temperature accelerates the crystallization of Cr_2O_3. In addition, the full width at half maximum (FWHM) of the Cr_2O_3-SP samples decreased with an increase in the pyrolysis temperature, which indicates an increase in the crystallite size.

The FT-IR absorption spectra of the prepared Cr_2O_3 samples are shown in Fig. 3. All samples show similar FT-IR patterns. The peak at approximately 1,640 cm^{-1} is attributed to adsorbed water on the surface of Cr_2O_3 [23]. The vibrational modes observed at 420, 558, and 640 cm^{-1} are attributed to Cr-O stretching [15,22,23]. The formation mechanism of Cr_2O_3 from the decomposition of $Cr(NO_3)_3 \cdot 9H_2O$ at high temperature (>120 °C) has been previously proposed [11]:

$$2Cr(NO_3)_3 \cdot 9H_2O \rightarrow Cr_2O_3 + 3/2\ O_2 + 6NO_2 + 18H_2O \quad (1)$$

Fig. 4(a1)-(d3) shows the SEM images of Cr_2O_3 samples with different magnifications, which were prepared by different preparation methods and conditions. As presented, Cr_2O_3-Cal-400 shows agglomerated particles with highly irregular shapes [Figs. 4(a1)-(a3)]. In contrast, all samples produced from spray pyrolysis maintained spherical shapes without agglomeration and had particle sizes of 0.5-1 μm. The surface morphologies of Cr_2O_3-SP samples are different depending on the addition of CTAB [Fig. 4(b) vs. Fig. 4(c)]. When the Cr_2O_3 particles were prepared without CTAB (Cr_2O_3-SP-400-0), they exhibited a densely packed structure, consisting of large primary particles of 50-100 nm [Fig. 4(b)]. However, the Cr_2O_3 particles prepared with CTAB (Cr_2O_3-SP-400-2 and Cr_2O_3-SP-800-2) exhibited a rough surface with many pores on the entire structure [Figs. 4(c1)-(d3)]. These pores were formed during the post-heating treatment process owing to the removal of carbonaceous materials that were produced from the decomposition of CTAB during the pyrolysis step under the N_2 atmosphere. The spherical particles obtained with CTAB consisted of smaller particles (20-50 nm), and their surface roughness was considerably increased compared to that of the Cr_2O_3-SP sample obtained without CTAB. The difference in morphologies occurred because the addition of an organic additive (CTAB) inhibits the growth of Cr_2O_3 crystals during the pyrolysis process [11,17]. This suggests that nanostructured Cr_2O_3 spheres can be produced by ultrasonic spray pyrolysis with the assistance of the organic additive. Recently, Pei et al. [17] reported that the sphere-like Cr_2O_3 was successfully produced by hydrothermal synthesis with the assistance of CTAB as a surfactant. However, the obtained Cr_2O_3 had a considerably larger particle size (>16 μm) without nanostructures on the surface [17]. This difference indicates that the morphology, particle size, and pore structure of the produced Cr_2O_3 particles were strongly affected by the preparation method.

Fig. 5(a) and (b) show the N_2 adsorption-desorption isotherms

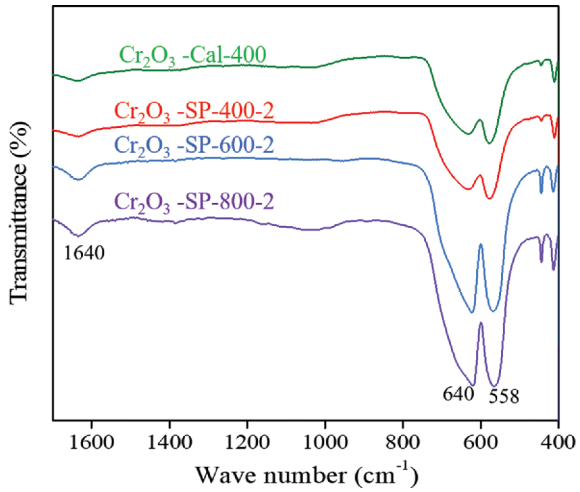

Fig. 3. FT-IR spectra of Cr_2O_3 samples obtained by different methods and synthesis conditions.

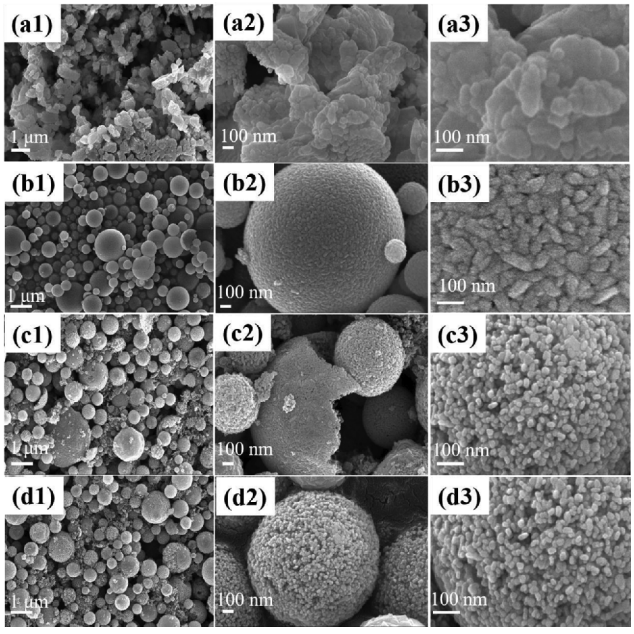

Fig. 4. FE-SEM images at different magnifications of ((a1), (a2), (a3)) Cr_2O_3-Cal-400, ((b1), (b2), (b3)) Cr_2O_3-SP-400-0, ((c1), (c2), (c3)) Cr_2O_3-SP-400-2, and ((d1), (d2), (d3)) Cr_2O_3-Cal-800-2.

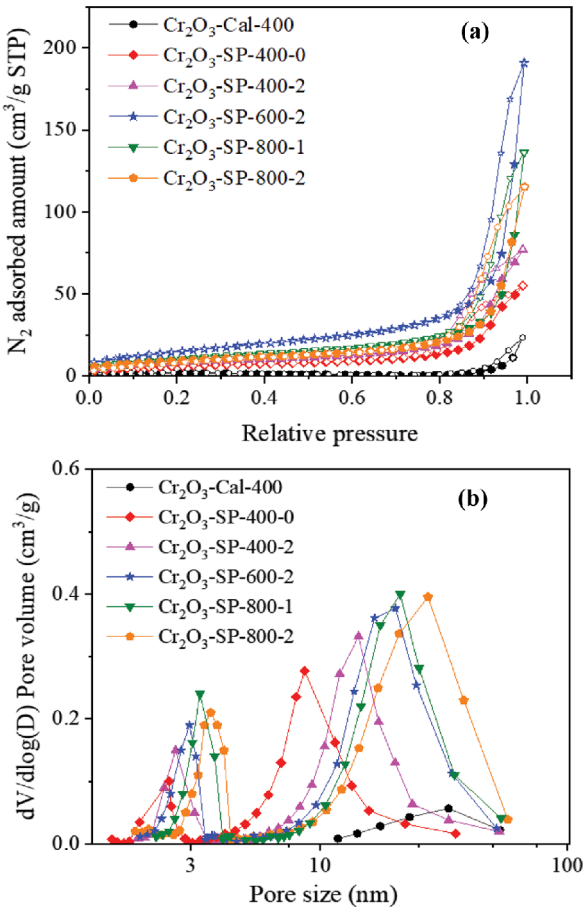

Fig. 5. Textural properties of Cr_2O_3 prepared by different methods and synthesis conditions: (a) N_2 adsorption-desorption isotherms and (b) pore size distributions.

Table 1. Textural properties of Cr_2O_3 prepared at different conditions

Sample	S_{BET}, m^2/g	Pore volume, cm^3/g	Pore size, nm
Cr_2O_3-Cal-400	3.5	0.04	30.2
Cr_2O_3-SP-400-0	26	0.10	8.1
Cr_2O_3-SP-400-2	52	0.30	14.2
Cr_2O_3-SP-600-2	48	0.21	16.2
Cr_2O_3-SP-800-1	31	0.11	17.4
Cr_2O_3-SP-800-2	42	0.18	17.9

and pore size distributions of the synthesized Cr_2O_3 particles. All nitrogen adsorption-desorption isotherms are of type IV (IUPAC classification) with a type-H3 hysteresis loop, which suggests the mesoporous characteristic of the prepared Cr_2O_3 samples. The Cr_2O_3-Cal-400 sample shows a much lower N_2 adsorbed amount compared to the Cr_2O_3-SP samples. Fig. 5(b) shows pore size distributions of Cr_2O_3-Cal and Cr_2O_3-SP samples. The Cr_2O_3-Cal-400 exhibits mono-modal pores in the range of 12-50 nm. However, for Cr_2O_3-SP samples, there are bi-modal pores. The smaller pore mode in the range of 2.5-3.5 nm is attributed to the mesoporous channels, while the larger pore mode may be formed owing to the interspace between the Cr_2O_3 secondary particles [13]. It is observed that the pore size is strongly affected by both CTAB concentration and pyrolysis temperature. At the same pyrolysis temperature of 400 °C, the addition of CTAB increased the pore size distribution of Cr_2O_3, which indicates an increase in the pore size. With an increase in the pyrolysis temperature from 400 °C to 800 °C, the pore size and pore size distribution also increased.

Table 1 shows the BET surface area, pore volume, and mean pore size of all Cr_2O_3 samples. The addition of CTAB to the Cr_2O_3-SP samples increased surface area, pore volume, and pore size compared to the pristine Cr_2O_3-SP sample. A similar result was reported by Li et al. [11], who investigated the effects of citric acid on the structure of Cr_2O_3 during the thermal decomposition process. With increasing pyrolysis temperature, the surface area and pore volume of the Cr_2O_3 samples decreased, while the average pore size increased. This result was obtained owing to the crystal growth of the Cr_2O_3 samples with an increase in the pyrolysis temperature [22]. This result is consistent with that of the XRD analysis. Among the prepared samples, Cr_2O_3-SP-400-2 shows the highest surface

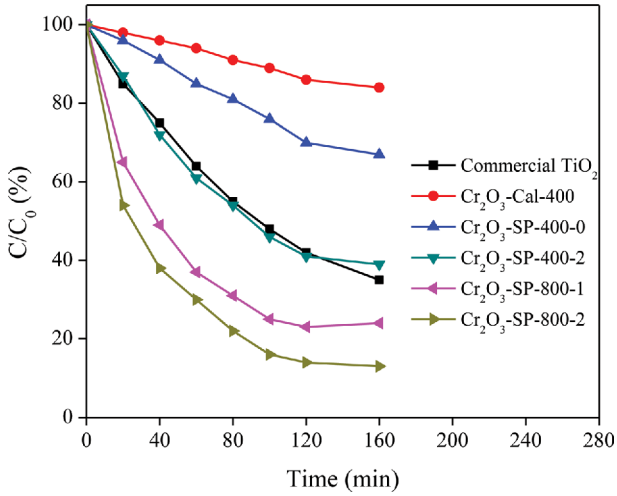

Fig. 7. Photocatalytic degradation of MO in an aqueous solution by the prepared Cr_2O_3 samples.

area of 52 m^2/g. This value is higher than that of Cr_2O_3 samples prepared by the thermal decomposition of the chromium complex (~21 m^2/g) [10], hydrothermal reduction of chromium anhydride in C_2H_5OH (~39 m^2/g) [18], wet chemical synthesis of porous Cr_2O_3 (34 m^2/g) [2], and commercial Cr_2O_3 (~32 m^2/g).

It has been observed that the addition of CTAB as a template resulted in the formation of mesopores throughout spherical Cr_2O_3-SP particles. The formation mechanism of mesoporous Cr_2O_3 spheres is proposed in Fig. 6. The precursor solution was prepared by mixing chromium salt and CTAB, which formed the CTAB-$Cr(NO_3)_3$ composite by the interactions of hydrogen bonds and electrostatic charges. Under the ultrasonic spray condition, small droplets were nebulized from the solution containing a well-dispersed precursor solution. During the spray pyrolysis process in the N_2 atmosphere, the CTAB-$Cr(NO_3)_3$ composite was decomposed to produce Cr_2O_3 and carbonaceous products (denoted as C_x for simplicity) (Fig. S1). The use of CTAB as an organic additive facilitated the effective dispersion of chromium salt as well as the inhibition of the crystal growth. After spray pyrolysis, the obtained spherical particles contained a large amount of carbonaceous products (C_x), which were further removed by post-heat treatment at 400 °C in the air. During this process, more porous structures

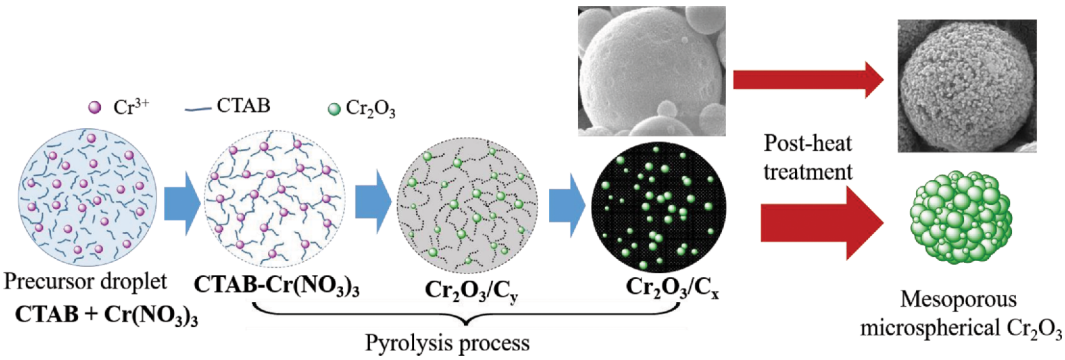

Fig. 6. Mechanism of the formation of mesoporous Cr_2O_3 microspheres by spray pyrolysis.

were formed owing to the elimination of carbonaceous materials.

Fig. 7 shows the photocatalytic degradation efficiency of MO over the prepared Cr_2O_3 catalysts and commercial TiO_2 (P25) for comparison. The Cr_2O_3-Cal sample shows considerably lower photocatalytic degradation efficiency than the Cr_2O_3-SP samples probably owing to the lower surface area. It has been observed that the addition of CTAB to the Cr_2O_3-SP catalysts strongly affects the degradation efficiency. For example, the Cr_2O_3-SP-400-2 and Cr_2O_3-SP-800-2 samples show much higher MO degradation efficiency than that of the Cr_2O_3-S-400-0 and Cr_2O_3-SP-800-1 samples, respectively. This is attributed to the differences in their porosities, which can determine the efficiency of the photocatalyst [8]. As mentioned, the addition of higher CTAB concentration to the Cr_2O_3-SP samples resulted in higher surface area and pore volume. The Cr_2O_3-SP-800 samples show considerably higher photocatalytic degradation efficiency than that of the Cr_2O_3-SP-400 sample, although they have a lower surface area and pore volume. This indicates that photocatalytic activity increased with an increase in the crystallinity of catalysts; this is consistent with the previous report on the photocatalytic efficiency of Cr_2O_3 [24]. The photocatalytic degradation efficiency of commercial TiO_2 was observed to be comparable to that of the Cr_2O_3-SP-400-2 sample, but much lower than that of both Cr_2O_3-SP-800-1 and Cr_2O_3-SP-800-2 catalysts.

CONCLUSION

Mesoporous Cr_2O_3 microspheres with controlled pore structures were fabricated by spray pyrolysis. The porosity and crystallinity of the synthesized microspherical Cr_2O_3 were controlled by the CTAB concentration and pyrolysis temperature. By adjusting the concentration of the surfactant during synthesis, the surface area and the pore size distribution of mesoporous Cr_2O_3 microspheres can be tuned. The photocatalytic degradation of methyl orange was determined to be dependent on both the porosity and crystallinity of the prepared Cr_2O_3. The highest photocatalytic degradation of ~90% was observed for Cr_2O_3 microspheres obtained at the pyrolysis temperature of 800 °C and the CTAB/Cr^{3+} molar ratio of 2. These findings suggest that spray pyrolysis is a potential method for the large scale production of mesoporous Cr_2O_3 microspheres.

ACKNOWLEDGEMENT

This study was supported by the Engineering Research Center of Excellence Program of the Korea Ministry of Science, ICT & Future Planning (MSIP)/National Research Foundation of Korea (NRF) (Grant NRF-2014R1A5A1009799).

SUPPORTING INFORMATION

Additional information as noted in the text. This information is available via the Internet at http://www.springer.com/chemistry/journal/11814.

REFERENCES

1. A. K. Adepu, S. Goskula, S. Chirra, S. Siliveri, S. R. Gujjula and N. Venkatathri, *J. Porous Mater.*, **26**, 1259 (2019).
2. S. Ayyappan, N. Ulagappan and C. N. R. Rao, *J. Mater. Chem.*, **6**, 1737 (1996).
3. B. Bai, P. Wang, L. Wu, L. Yang and Z. Chen, *Mater. Chem. Phys.*, **114**, 26 (2009).
4. Y. K. Bai, R. T. Zheng, Q. Gu, J. J. Wang, B. S. Wang, G. A. Cheng and G. Chen, *J. Mater. Chem. A.*, **2**, 12770 (2014).
5. L. Chen, Z. Song, X. Wang, S. V. Prikhodko, J. Hu, S. Kodambaka and R. Richards, *ACS Appl. Mater. Interfaces*, **1**, 1931 (2009).
6. J. S. Cho, K. Y. Jung and Y. C. Kang, *Phys. Chem. Chem. Phys.*, **17**, 1325 (2015).
7. Y. H. Cho, Y. N. Ko, Y. C. Kang, I.-D. Kim and J.-H. Lee, *Sens. Actuator B-Chem.*, **195**, 189 (2014).
8. J. Choi, K. S. Yoo and J. Kim, *Korean J. Chem. Eng.*, **35**, 2480 (2018).
9. N. A. Dhas, Y. Koltypin and A. Gedanken, *Chem. Mater.*, **9**, 3159 (1997).
10. R. F. K. Gunnewiek, C. F. Mendes and R. H. G. A. Kiminami, *Mater. Lett.*, **129**, 54 (2014).
11. L. Li, Z. F. Yan, G. Q. Lu and Z. H. Zhu, *J. Phys. Chem. B.*, **110**, 178 (2006).
12. M. D. Lima, R. Bonadimann, M. J. de Andrade, J. C. Toniolo and C. P. Bergmann, *J. Eur. Ceram. Soc.*, **26**, 1213 (2006).
13. H. Liu, X. Du, X. Xing, G. Wang and S. Z. Qiao, *Chem. Commun.*, **48**, 865 (2012).
14. J. Ma, J. Ding, L. Yu, L. Li, Y. Kong and S. Komarneni, *Appl. Clay Sci.*, **107**, 85 (2015).
15. M. Ocaña, *J. Eur. Ceram. Soc.*, **21**, 931 (2001).
16. S.-W. Park, O.-S. Joo, K.-D. Jung, H. Kim and S.-H. Han, *Korean J. Chem. Eng.*, **17**, 719 (2000).
17. Z. Pei, X. Gao, Y. Zhang and X. Lu, *Mater. Lett.*, **116**, 215 (2014).
18. Z. Pei, H. Xu and Y. Zhang, *J. Alloys Compd.*, **468**, L5 (2009).
19. Z. Pei, X. Zheng and Z. Li, *J. Nanosci. Nanotechnol.*, **16**, 4655 (2016).
20. S. R. Pratap, M. Shyamsundar and S. Z. M. Shamshuddin, *J. Porous Mater.*, **25**, 1265 (2018).
21. D. Rafi-ud, Q. Xuanhui, L. Ping, L. Zhang, W. Qi, M. Z. Iqbal, M. Y. Rafique, M. H. Farooq and D. Islam-ud, *J. Phys. Chem. C.*, **116**, 11924 (2012).
22. M. Roy, S. Ghosh and M. K. Naskar, *Mater. Chem. Phys.*, **159**, 101 (2015).
23. B. T. Sone, E. Manikandan, A. Gurib-Fakim and M. Maaza, *Green. Chem. Lett. Rev.*, **9**, 85 (2016).
24. J. Su, H. Xue, M. Gu, H. Xia and F. Pan, *Ceram. Int.*, **40**, 15051 (2014).
25. F. Subhan, S. Aslam, Z. Yan, M. Khan, U. J. Etim and M. Naeem, *J. Porous Mater.*, **26**, 1465 (2019).
26. S. C. Tsai, Y. L. Song, C. S. Tsai, C. C. Yang, W. Y. Chiu and H. M. Lin, *J. Mater. Sci.*, **39**, 3647 (2004).
27. T. Valdés-Solís and A. B. Fuertes, *Mater. Res. Bull.*, **41**, 2187 (2006).
28. N. Venugopal, W.-S. Kim and K. Y. Sohn, *Korean J. Chem. Eng.*, **36**, 1536 (2019).
29. T. K. Vo, W.-S. Kim, S.-S. Kim, K. S. Yoo and J. Kim, *Energy Convers. Manag.*, **158**, 92 (2018).
30. D. Vollath, D. V. Szabó and J. O. Willis, *Mater. Lett.*, **29**, 271 (1996).
31. C. Yeom and Y. Kim, *Korean J. Chem. Eng.*, **35**, 587 (2018).
32. Y. Zhang, Y. Xu, T. Li and Y. Wang, *Particuology*, **10**, 46 (2012).